

# Evaluation of Single-Photon Emission Computed Tomography Myocardial Perfusion Detection Capability through Physical Descriptors

---

Dundara Debeljuh, Dea; Matheoud, Roberta; Pribanić, Ivan; Brambilla, Marco; Jurković, Slaven

Source / Izvornik: **Applied Sciences**, 2024, 14

Journal article, Published version

Rad u časopisu, Objavljena verzija rada (izdavačev PDF)

<https://doi.org/10.3390/app14125283>

Permanent link / Trajna poveznica: <https://um.nsk.hr/um:nbn:hr:184:610519>

Rights / Prava: [Attribution 4.0 International](#)/[Imenovanje 4.0 međunarodna](#)

Download date / Datum preuzimanja: **2025-02-19**







Repository / Repozitorij:

[Repository of the University of Rijeka, Faculty of Medicine - FMRI Repository](#)



## Article

# Evaluation of Single-Photon Emission Computed Tomography Myocardial Perfusion Detection Capability through Physical Descriptors

Dea Dundara Debeljuh <sup>1,2,3</sup>, Roberta Matheoud <sup>4</sup>, Ivan Pribanić <sup>1,3</sup>, Marco Brambilla <sup>4</sup>  
and Slaven Jurković <sup>1,3,\*</sup>

<sup>1</sup> Medical Physics Department, University Hospital Rijeka, 51000 Rijeka, Croatia; dea.dundara.debeljuh@kbc-rijeka.hr (D.D.D.)

<sup>2</sup> Department of Radiology, General Hospital Pula, 52100 Pula, Croatia

<sup>3</sup> Department of Medical Physics and Biophysics, Faculty of Medicine, University of Rijeka, 51000 Rijeka, Croatia

<sup>4</sup> Department of Medical Physics, University Hospital "Maggiore della Carità", 28100 Novara, Italy

\* Correspondence: slaven.jurkovic@medri.uniri.hr; Tel.: +385-51-658-599

**Abstract:** A comprehensive validation of data acquired by different myocardial perfusion imaging (MPI) systems was performed to evaluate contrast, self-attenuation properties, and perfusion detection capability. An anthropomorphic phantom with a myocardial insert and perfusion defect was used to simulate <sup>99m</sup>Tc-tetrofosmin distribution. Different MPI systems were evaluated: a SPECT system with iterative reconstruction algorithms and resolution recovery (IRR) with/without scatter correction (SPECT-IRR-SC and SPECT-IRR), and a cardio-centric IQ SPECT/CT system with IRR, with/without scatter and attenuation corrections (IQ-IRR-SC-AC and IQ-IRR). The image quality was assessed through physical descriptors: the contrast between the left ventricular (LV) wall and LV inner chamber ( $C_{LV/LVIC}$ ), intrinsic contrast (IC), and net contrast (NC).  $C_{LV/LVIC}$  was found to be superior for IQ-IRR-SC-AC. The IC results showed non-uniformity of the signal intensity in the LV wall for the SPECT systems. The lowest IC values were obtained for IQ-IRR-SC-AC, except for septal position, where an underestimation of the signal intensity was revealed. The NC was found to be the highest for IQ-IRR-SC-AC and SPECT-IRR-SC. Additionally, for IQ-IRR-SC-AC, the NC increased in posterior and septal positions compared to IQ-IRR, enabling better perfusion detection capability over short-axis images. IQ-IRR showed performances comparable to SPECT-IRR. The characterization and evaluation perfusion detection capability of the MPI systems enabled the investigation of the systems' performance and limitations.

**Keywords:** medical physics; SPECT; hybrid imaging; myocardial perfusion imaging; image quality; scatter correction; attenuation correction; iterative reconstruction with resolution recovery



**Citation:** Dundara Debeljuh, D.; Matheoud, R.; Pribanić, I.; Brambilla, M.; Jurković, S. Evaluation of Single-Photon Emission Computed Tomography Myocardial Perfusion Detection Capability through Physical Descriptors. *Appl. Sci.* **2024**, *14*, 5283. <https://doi.org/10.3390/app14125283>

Academic Editor: Laura Cerenelli

Received: 17 May 2024

Revised: 10 June 2024

Accepted: 12 June 2024

Published: 18 June 2024



**Copyright:** © 2024 by the authors. Licensee MDPI, Basel, Switzerland. This article is an open access article distributed under the terms and conditions of the Creative Commons Attribution (CC BY) license (<https://creativecommons.org/licenses/by/4.0/>).

## 1. Introduction

The application of physics in nuclear cardiology aims to improve the quality of the image data obtained using different combinations of tomographic systems, reconstruction algorithms, and corrections used in myocardial perfusion imaging (MPI). The characterization of imaging systems and the evaluation of image data through the application of formalisms and metrics of radiation physics is crucial for the investigation of system performance and the determination of possible limitations.

MPI is a non-invasive tomographic nuclear medicine procedure dedicated to identifying early asymptomatic coronary artery disease (CAD) or examining the clinical impact of previously diagnosed CAD. Single-photon emission computed tomography (SPECT) is used to assess the blood flow through the myocardium, and to locate areas where it is diminished by stenosed or obstructed coronary arteries, i.e., areas of perfusion defects. The

blood flow information is obtained by the analysis of radiopharmaceutical accumulation and distribution in the myocardium. Therefore, the quality of the image data and the capability of the system to detect PDs are essential.

Image quality is related to system performance and can be expressed by several physical parameters. The most important are related to the imaging system, i.e., contrast, spatial resolution, sensitivity, and uniformity [1–7]. When performing MPI on a SPECT system with NaI-crystal and parallel-hole collimators, only a small portion of the detector area is used. In addition, the loss of spatial resolution due to source-to-detector distance when using parallel-hole collimators must be considered. Cardio-centric acquisition and multi-focal collimators have improved the sensitivity and resolution of NaI-crystal detector systems by the specific convergent collimator geometry in the center of the detector area. Moreover, they have allowed the acquisition time or the administered activity to be reduced [8–11].

The performance of systems with NaI-crystal detectors has been further enhanced by the introduction of iterative reconstruction algorithms with resolution recovery (IRR). These algorithms enable three-dimensional collimator response function modeling and account for the spatial resolution of the system in the reconstruction process [1,12–15]. Collimator response function modeling is performed using the physical and geometric features of the detector and collimator along with orbit shape, detector rotation radius, and patient–detector distance to improve the accuracy of the radiopharmaceutical distribution visualization on reconstructed images [1,16]. Resolution recovery is particularly important for MPI procedures, where the change in the position of the organ can cause reconstruction artifacts due to differences in spatial resolution [17]. In addition, IRR algorithms allow the correction of various degrading factors such as noise, scatter, and attenuation [1,13–15]. The contribution of the scattered gamma rays originating in adjacent organs can be corrected using multiple energy windows that enable scatter contribution estimation during IRR and compensation for it [18,19]. Gamma ray attenuation in tissues can be corrected using transmission data acquired through computed tomography (CT). Although mandatory for some cardio-centric systems [13], this is still an open question due to the possible mismatch between emission and transmission data that may result in attenuation correction (AC)-induced artifacts [17].

A comprehensive characterization of nuclear cardiology imaging systems should include the evaluation of system diagnostic performance in terms of perfusion detection capability. The aim of this study was to quantify self-attenuation characteristics, non-uniformities of the signal intensity and maximum contrast between the perfusion defect (PD) and the LV wall for nuclear cardiology imaging systems, in reproducible and controlled clinical conditions with an anthropomorphic SPECT phantom. Therefore, a set of physical descriptors determined to validate the contrast on reconstructed images was used: the contrast between the LV wall and LV inner chamber ( $C_{LV/LVIC}$ ), the intrinsic contrast (IC), and the net contrast (NC). The evaluation involved a SPECT device with parallel-hole low-energy high-resolution (LEHR) collimators, a non-circular detector orbit and IRR reconstruction algorithm with/without scatter correction (SC), and a cardio-centric SPECT/CT device with multifocal collimators, IRR and with/without SC, and AC. The image analysis was performed in order to evaluate and quantify the level of uniformity of the perfusion detection capability of the nuclear cardiology imaging system over the LV wall. A comparison between the different systems in terms of detection performance was performed. The maximum contrast values between the PD and the LV wall for each system were used as reference values for system characterization.

## 2. Materials and Methods

### 2.1. MPI Systems

Different imaging device–reconstruction algorithm–correction combinations were considered. For data acquisition the following imaging devices were used: two SPECT/CT Symbia T2 devices (Siemens Healthineers, Erlangen, Germany) with low-energy high-resolution (LEHR) collimators, and one cardio-centric SPECT/CT Symbia Intevo Excel

(Siemens Healthineers, Erlangen, Germany) and one cardio-centric Symbia Intevo device, both with IQ SPECT and SmartZoom collimators. Clinical acquisition protocols were used (Table 1). Reconstruction parameters were selected according to the recommended algorithm settings. The acquisition protocol for the Symbia T2 included SPECT imaging only. Raw SPECT data were reconstructed with the IRR algorithm (Flash3D, Siemens Medical Solutions). A double-energy window was used for imaging, allowing the implementation of the SC. Reconstruction settings were selected based on the matrix size, pixel size, and number of projections used for acquisitions: 15 iterations, 8 subsets and a 13.2 mm Gaussian post-filter (pixel size 6.6 mm).

**Table 1.** Acquisition and reconstruction protocol details.

Imaging Device	Symbia T2	Symbia Intevo/Intevo Excel
Collimator	LEHR	SmartZoom
Matrix size	64 × 64	128 × 128
Zoom	1.45	1
Pixel size	6.6	4.8
Detectors	Both detectors	Both detectors
Number of projections	64	34
Starting angle	45	59
Degrees of rotation	90	104
Detector configuration	90	76
Detector orbit	Non-Circular	Cardio-Centric
Acquisition mode	Step and shoot	Step and shoot
Energy window	Dual-energy window: photopeak and lower scatter	Dual-energy window: photopeak and lower scatter
Reconstruction algorithm	Flash 3D IRR	IQ Flash 3D IRR
Corrections	SC No corrections	SC-AC No corrections

IQ SPECT data acquisition included both the SPECT and CT. The latter was performed using the following acquisition parameters: 130 kV, reference tube current exposure time product 55 mAs (Care Dose 4D, Siemens Healthineers), collimation 2 × 4 mm, pitch 1.0, slice 5 mm. The image data obtained by this device were reconstructed with IRR algorithm IQ Flash 3D with 10 iterations, 3 subsets and 10 mm FWHM Gaussian post-filter (pixel size 4.8 mm), either with both SC and AC or correction-free.

Overall, four different imaging device–reconstruction algorithm–correction combinations, hereinafter referred as *MPI systems*, were evaluated: SPECT with IRR (SPECT-IRR), SPECT with IRR and SC (SPECT-IRR-SC), cardio-centric IQ SPECT with IRR, SC, and AC (IQ-IRR-SC-AC), and correction-free cardio-centric IQ SPECT with IRR (IQ-IRR).

## 2.2. Anthropomorphic Phantom

An anthropomorphic thorax phantom (Figure 1) with inserts that mimic the myocardium, lungs, liver, and spinal cord was used (Torso Phantom<sup>TM</sup> with Cardiac Insert<sup>TM</sup>, Data Spectrum Corporation, Hillsborough, NC, USA). The myocardial insert (Figure 1b) consists of a fillable chamber that mimics the LV wall and the LV inner chamber (LVIC). To simulate pathological myocardial perfusion conditions, an insert filled with water (“cold insert”) was used. This simulates a PD in predefined positions inside the myocardial wall. A PD insert with specific dimensions was used (Figure 1c): coverage angle on a short-axis plane of 45°, 2 cm over the long-axis plane (45° × 2 cm). The myocardial insert, liver, and torso were filled with <sup>99m</sup>Tc solution of different activity concentrations, as detailed below

(Table 2). The lung insert filled with Styrofoam® beads and water mimicked low-density lung tissue. The spinal cord insert was made of Teflon®.

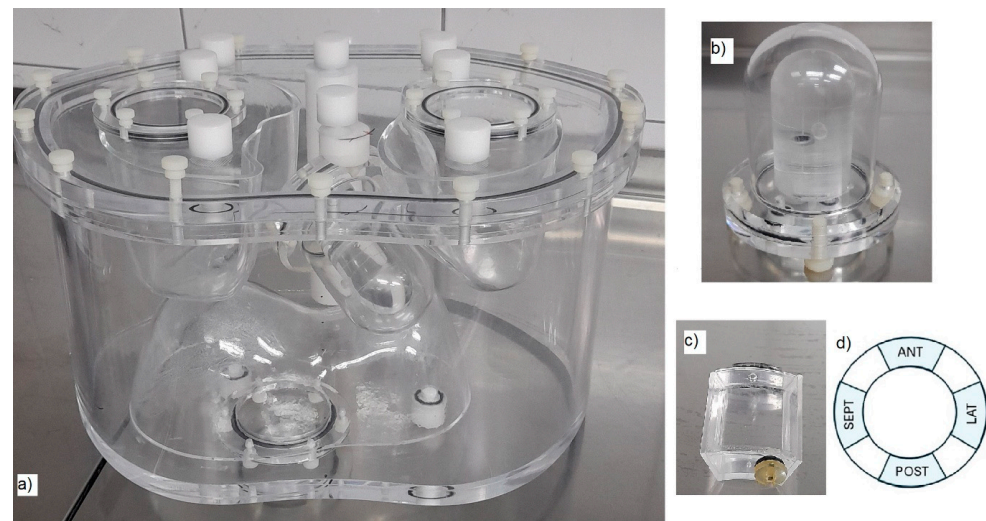


**Figure 1.** (a) Anthropomorphic thorax phantom; (b) myocardial insert; (c) perfusion defect insert; (d) positions of the PD in the short-axis plane.

The volumes of the different compartments were determined experimentally to be able to determine the required activity. These data are essential to obtain the required activity concentrations based on the distribution of the radiopharmaceutical in the body.

### 2.3. Experimental Session

Data acquisitions were performed for two simulated myocardial wall perfusion conditions: normal and pathological. In normal perfusion simulations, the anthropomorphic phantom was filled with  $^{99m}\text{Tc}$  solution of different activity concentrations (Table 2) using the formalism reported by Zoccarato et al. [1] to simulate the distribution of the radiopharmaceutical  $^{99m}\text{Tc}$ -tetrofosmin in the body.

**Table 2.** Activity concentration values for different inserts used in the preparation of the phantom.

Insert	Volume (mL)	Activity (MBq)	Activity Concentration (MBq/mL)	Activity Concentration Ratio with Respect to Chest
LV wall	122.88	10.3	0.083	20.4
Inner chamber	64.70	0.3	0.004	1.0
Liver	1308.90	65.2	0.050	12.2
Chest	9050.00	37.0	0.004	-

In pathological perfusion simulations, a *PD* insert filled with water was used to simulate a transmural defect located in the middle of the *LV* wall. The phantom was prepared with the same activity concentrations used in the normal myocardial wall perfusion simulations (Table 2). Acquisitions were performed with the perfusion defect in four wall positions: anterior, lateral, posterior, and septal (Figure 1d).

Phantom images were acquired to obtain a proper level of count statistics:  $3 \times 10^6$  counts for SPECT acquisitions and  $10^6$  counts for IQ SPECT acquisitions [1,20]. The phantom was positioned according to the MPI clinical patient positioning protocol of each investigated *MPI system* to simulate patient position during clinical myocardial perfusion imaging: supine position, feet first. In the case of the cardio-centric IQ SPECT device, the myocardial insert was positioned within the region of the highest magnification of the multifocal collimators [8]. Standard clinical acquisition protocols were used as detailed in Table 1.

The reconstruction process was performed to obtain transaxial slices for each *MPI system*. The transaxial slices were realigned according to cardiac orientation to obtain short-axis slices.

#### 2.4. Image Data

The raw image data (projections) acquired using the four imaging devices were reconstructed and realigned using Siemens syngo.via software for molecular imaging (Siemens Healthineers, Erlangen, Germany, <https://www.siemens-healthineers.com/digital-health-solutions/syngovia> accessed on 10 June 2024). Short-axis images were exported in DICOM format and used for image analysis. The phantom imaged data are the authors' property and can be used and shared by the authors.

#### 2.5. Image Analysis

A comprehensive image quality evaluation was performed by analyzing a set of physical image quality descriptors to assess and compare the performance of different *MPI systems*. The contrast was evaluated through the contrast between the *LV* wall and the *LV* inner chamber, the contrast of the *PD* with respect to the *LV* wall, the intrinsic contrast, and the net contrast. The Fiji edition of ImageJ open-source software, (National Institutes of Health, Bethesda, MD, USA) for processing and analyzing image data, version 2.14.0/1.54 f, was used. In ImageJ, the short-axis images were opened as a 32-bit file. The regions of interest were drawn using the freehand option. The mean number of counts in the regions of interest were used in the calculation of the descriptors. In ImageJ, when displaying short-axis images, the lookup table (LUT) "cool" was applied.

The contrast between the *LV* wall and the *LV* inner chamber (*LVIC*) was defined as the percentage of the ratio between the contrast measured on the reconstructed images ( $C_{LV/LVIC,meas}$ ) and the contrast defined by the preparation of the phantom ( $C_{LV/LVIC,phantom}$ ):

$$C_{LV/LVIC}(\%) = \frac{C_{LV/LVIC,meas}}{C_{LV/LVIC,phantom}} \times 100 \quad (1)$$

$C_{LV/LVIC,meas}$  was determined as:

$$C_{LV/LVIC,meas} = \frac{\overline{\eta}_{LV} - \overline{\eta}_{LVIC}}{\overline{\eta}_{LV} + \overline{\eta}_{LVIC}} \quad (2)$$

where  $\overline{\eta}_{LV}$  and  $\overline{\eta}_{LVIC}$  are the mean number of counts per voxel in the *LV* wall and *LV* inner chamber, respectively, on the short-axis images of the normal heart [1] obtained through image analysis.  $C_{LV/LVIC,phantom}$  is a function of the activity concentrations in the *LV* wall and *LV* inner chamber,  $AC_{LV}$  and  $AC_{LVIC}$ , respectively.  $C_{LV/LVIC,phantom}$  was defined as:

$$C_{LV/LVIC,phantom} = \frac{AC_{LV} - AC_{LVIC}}{AC_{LV} + AC_{LVIC}} \quad (3)$$

The contrast of the *PD* with respect to the *LV* wall defined by the preparation of the phantom is:

$$C_{PD,phantom}(100\%) = \frac{AC_{LV} - AC_{PD}}{AC_{LV} + AC_{PD}} \times 100 \quad (4)$$

where  $AC_{LV}$  and  $AC_{PD}$  are the activity concentrations in the *LV* wall and in the *PD*, respectively [21]. In the simulation of a pathological heart, the perfusion defect is filled with water and the  $C_{PD,phantom} = 100\%$ . Thus, the contrast between the *PD* and the *LV* wall was determined as:

$$C_{PD}(\%) = \frac{\overline{\eta}_{LV} - \overline{\eta}_{PD}}{\overline{\eta}_{LV} + \overline{\eta}_{PD}} \times 100 \quad (5)$$

where  $\overline{\eta}_{LV}$  and  $\overline{\eta}_{PD}$  are the mean number of counts per voxel in the *LV* wall and perfusion defect of the pathological heart, respectively [21]. The contrast between the *PD* and the

LV wall was evaluated on the short-axis slices of the pathological heart where the PD was visible.

To estimate the intrinsic contrast of the MPI system due to self-attenuation, the contrast of the areas where the PD was positioned with respect to the LV wall was evaluated on the corresponding short-axis slices of the normal heart using the regions of interest (ROIs) used for  $C_{PD}(\%)$  evaluation:

$$IC(\%) = \frac{\overline{\eta}_{LV, norm} - \overline{\eta}_{PD, norm}}{\overline{\eta}_{LV, norm} + \overline{\eta}_{PD, norm}} \times 100 \quad (6)$$

where  $\overline{\eta}_{LV, norm}$  and  $\overline{\eta}_{PD, norm}$  are the mean counts per voxel in the LV wall of the normal heart and in the position corresponding to the perfusion defect, respectively [21].

Finally, for each type of MPI system and each PD position, the net contrast was determined as:

$$NC = C_{PD} - IC \quad (7)$$

NC is an image quality descriptor related to the perfusion detection capability of the MPI system. NC values should be used as reference values of the maximum contrast between the PD and the LV wall for each MPI system and different PD positions [21]. An ideal MPI system is considered self-attenuation-artifact-free, with  $IC = 0$ ; hence,  $C_{PD} = 100\%$  and, consequently,  $NC = 100\%$ .

## 2.6. Statistical Analysis

The influence of the MPI system on the contrast between the LV wall and the LV inner chamber was evaluated using a one-way main-effect ANOVA. The MPI system was considered as the independent variable, and the contrast between the LV wall and LV inner chamber as the dependent variable.

The impact of the MPI system and PD position on the net contrast were evaluated using a two-way main-effect ANOVA. The MPI system and lesion position were considered as independent variables, and the lesion net contrast was considered as the dependent variable.

If a significant F value was found for one independent variable, then this was referred to as a main effect. When a main effect was found, a post hoc test (Scheffe' test) was performed to compare the dependent variables upon the levels of the factor  $2 \times 2$ , thus identifying the main sources of variability.

The analysis was performed using Statistica version 12 (StatSoft Inc., Tulsa, OK, USA) with a two-sided type I error of  $p = 0.05$ . Least-square means and standard errors were calculated for all image quality descriptors.

The results from the two SPECT systems and the results from the two cardio-centric IQ SPECT systems were compared using a *t*-test for independent variables to test the possibility of pooling the results. The null hypothesis was that the mean values of the physical descriptors obtained by the same imaging devices were not significantly different.

## 3. Results

The *t*-test for independent variables used for the two SPECT systems and for the two IQ SPECT systems confirmed the null hypotheses. Therefore, the acquired data were pooled together. The results are shown for four MPI systems: SPECT-IRR, SPECT-IRR-SC, IQ-IRR-SC-AC, and IQ-IRR.

### 3.1. Contrast between LV Wall and LV Inner Chamber

The MPI system was a main effect with a statistically significant impact on the contrast between the LV wall and the LV inner chamber ( $F = 31.2$ ,  $p < 0.001$ ). A post hoc Scheffe test outlined the statistically significant differences, as shown in Figure 2. Statistically significant differences were found between all MPI systems, except between SPECT-IRR and IQ-IRR. The differences between the MPI systems in terms of image quality can be visually evaluated from Figure 3.

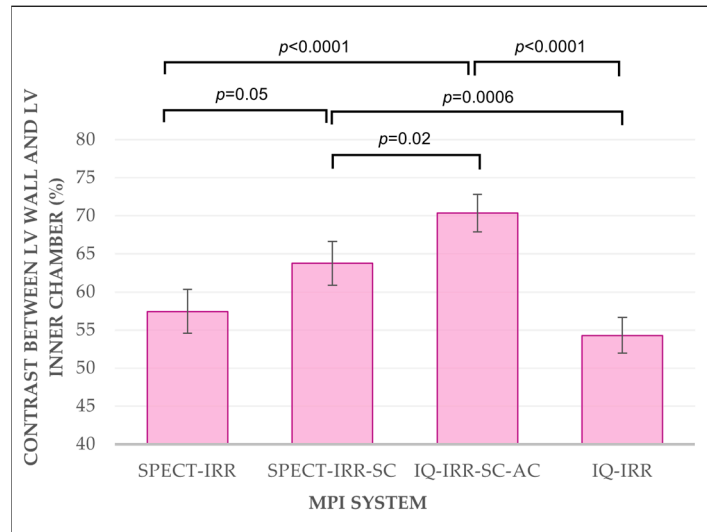


**Figure 2.** Contrast between LV wall and LV inner chamber values for different MPI systems. Values represent least-square averages; vertical bars represent 95% confidence intervals.

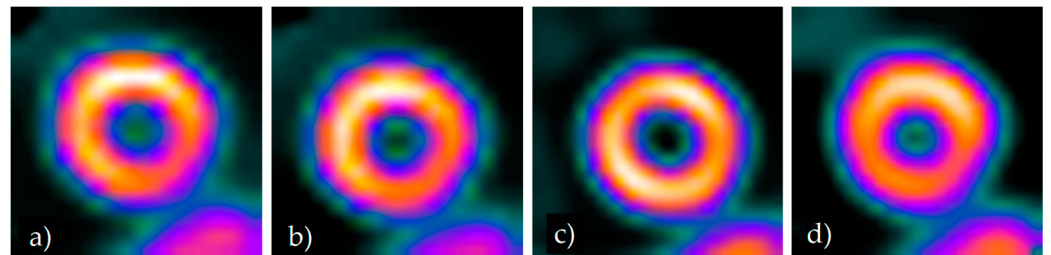


**Figure 3.** Short-axis images acquired with different MPI systems: (a) SPECT with IRR; (b) SPECT with IRR and SC; (c) IQ SPECT with IRR, SC, and AC; (d) correction-free IQ SPECT IRR.

### 3.2. Intrinsic Contrast

The intrinsic contrast values at four PD positions are shown in Figure 4 for each of the MPI systems evaluated.

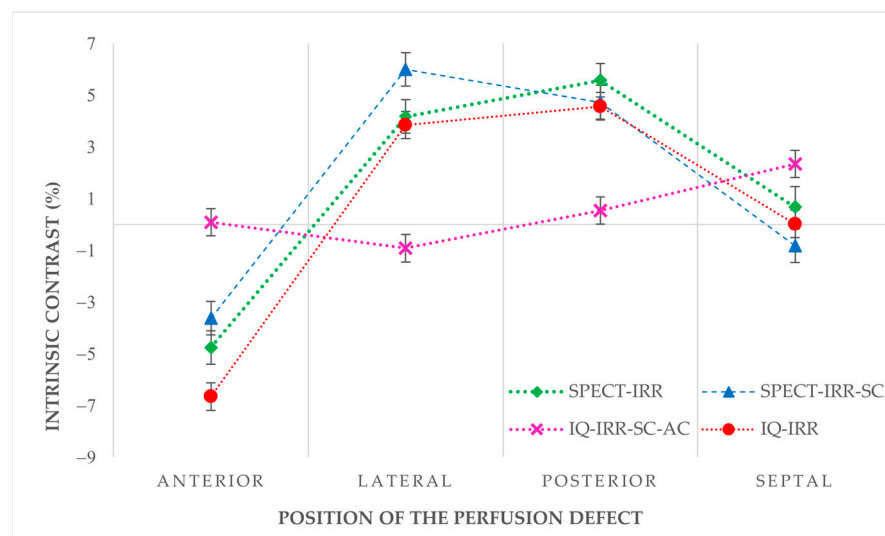


**Figure 4.** Intrinsic contrast values at anterior, lateral, posterior, and septal position of the myocardial wall for evaluated MPI systems. Values represent least-square average values; vertical bars represent 95% confidence intervals. For clarity, points are connected by dashed lines.



### 3.3. Net Contrast

The *MPI system* and lesion position were the main effects on the net contrast ( $F = 5.72$ ,  $p = 0.002$  and  $F = 37.23$ ,  $p < 0.001$ , respectively). A post hoc analysis outlined a statistically significant difference between the net contrast values for the *MPI system* pairs, as shown in Figure 5.

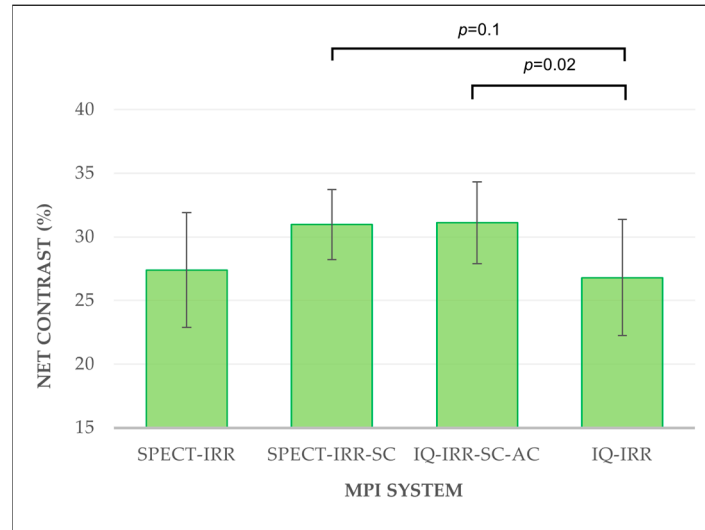


**Figure 5.** Net contrast values for different *MPI systems*. Values represent least-square average values; vertical bars represent 95% confidence intervals.

Statistically significant differences were found between SPECT-IRR-SC and IQ-IRR and IQ-IRR-SC-AC and IQ-IRR. The net contrast values at four *PD* positions are shown in Figure 6 for the *MPI systems* used.

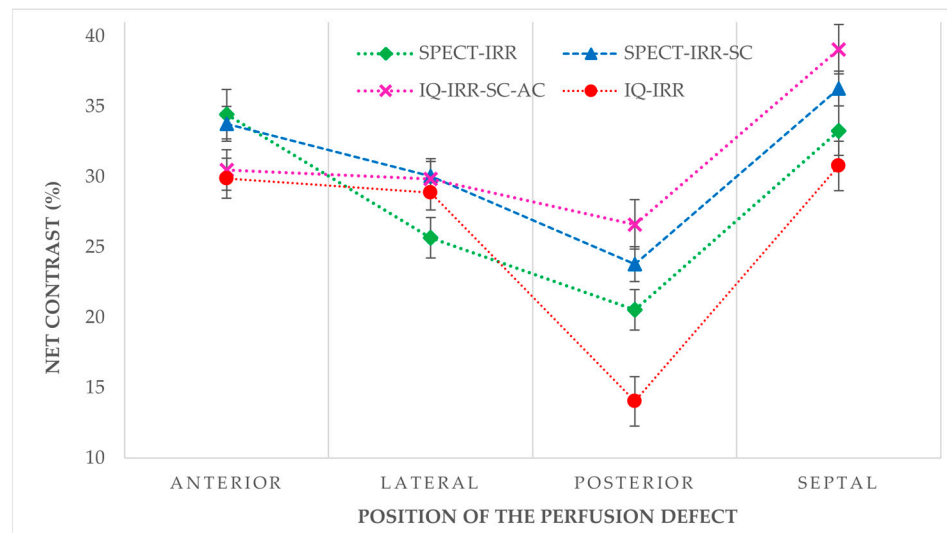


**Figure 6.** Net contrast values at anterior, lateral, posterior, and septal position of the myocardial wall for different *MPI systems*. Values represent least-square average values; vertical bars represent 95% confidence intervals. For clarity, points are connected by dashed lines.

A Scheffe post hoc analysis revealed a statistically significant difference between the mean net contrast values for different *MPI systems* at four *PD* positions. The weighted mean net contrast values for different lesion positions are shown in Figure 7.

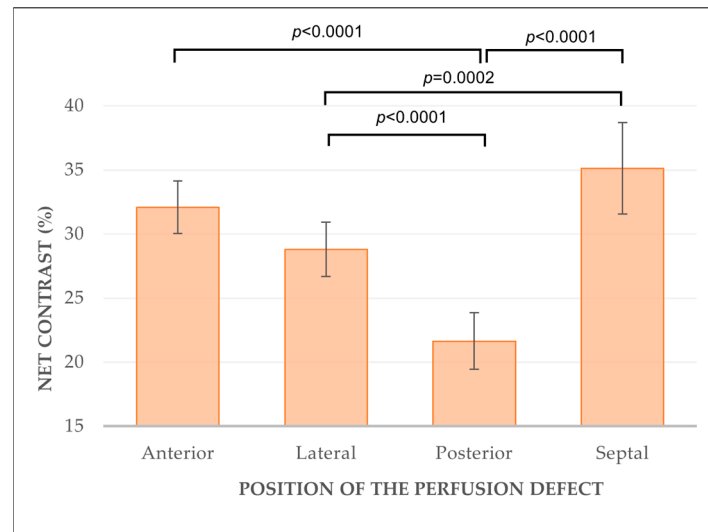


**Figure 7.** Net contrast values for different positions of the perfusion defect: anterior, lateral, posterior, septal. Values represent least-square average values; vertical bars represent 95% confidence intervals.

Figure 8 shows examples of short-axis images of the pathological heart with the PD in four positions.

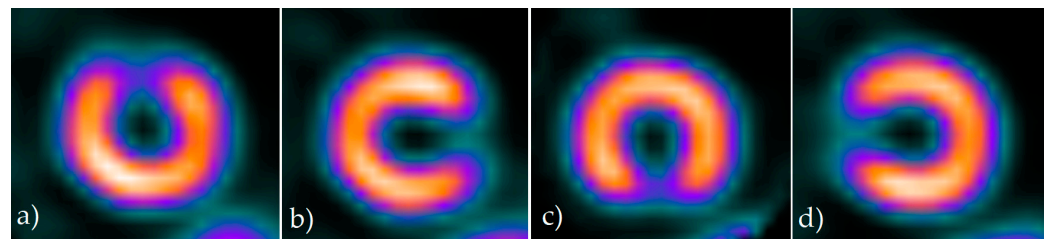


**Figure 8.** Short-axis images of the pathological heart obtained using IQ-IRR-SC-AC. Different PD positions are shown: (a) anterior; (b) lateral; (c) posterior; (d) septal.

#### 4. Discussion

The characteristics of the imaging devices, reconstruction algorithms, and corrections used for the MPI require a thorough image quality evaluation as part of the comprehensive characterization of imaging systems. Such image quality analysis consists of an evaluation through physical image quality descriptors to validate the performance of the MPI systems. In this investigation, the image quality of different MPI systems was studied by using specific image quality descriptors related to contrast, self-attenuation characteristics, and perfusion detection capability.

The contrast defined during the preparation of the phantom was  $C_{LV/LVIC,phantom} = 0.91$ . The differences in the  $C_{LV/LVIC}$  values between SPECT-IRR-SC and SPECT-IRR were statistically significant ( $63.8 \pm 1.4\%$  vs.  $57.4 \pm 1.4\%$ ). IQ-IRR-SC-AC was found to have a considerably higher  $C_{LV/LVIC}$  value ( $70.3 \pm 1.2\%$ ) than any of the other MPI systems investigated (Figure 2). This can also be seen in Figure 3c, where the LV inner chamber has the same signal intensity as the background, unlike in other MPI systems. If corrections are not used in IQ SPECT,  $C_{LV/LVIC}$  decreases by more than 15%. The same tendency was found by Caobelli et al. [10] who reported a higher contrast in IQ-IRR-SC-AC compared with IQ-IRR. However, they reported considerably higher values (~20%). The contrast values obtained by IQ-IRR and SPECT-IRR are not significantly different, which is in line with findings reported by Imbert et al. (2012) [2]. This result shows the superiority of IRR with SC and AC in combination with Smart Zoom collimators with respect to other MPI systems in terms of  $C_{LV/LVIC}$ .

The differences between *MPI systems* could be visually evaluated by comparing short-axis images (Figure 3). When using IQ-IRR-SC-AC (Figure 3c), the *LV* inner chamber can be easily recognized and *LV* walls appear thinner and with sharper borders. If corrections are not used for IQ systems (Figure 3d), the quality of the image data decreases in both contrast and spatial resolution. Between SPECT-IRR (Figure 3a) and SPECT-IRR-SC (Figure 3b), an improvement in the image quality due to applied correction for the scatter component can be observed.

A quantitative analysis of the self-attenuation characteristics of the *MPI system* was performed through the evaluation of the intrinsic contrast. The results were used to correct the measured contrast between the *PD* and the *LV* wall to obtain reference values of the maximum contrast for each *MPI system* and different *PD* positions. As far as the intrinsic contrast is concerned, an overestimation of the signal intensity ( $IC < 0$ ) in the anterior position and an underestimation ( $IC > 0$ ) of the signal intensity in the lateral and posterior position was observed for the majority of the investigated *MPI systems*, except for IQ-IRR-SC-AC (Figure 4). The non-uniformity of the signal intensity is more pronounced for SPECT-IRR-SC and IQ-IRR in the lateral and anterior position, respectively. The observed decrease in the signal intensity in the lateral and posterior positions for the majority of the *MPI systems* could be related to the farthest location of this area from the detector and correlated to the attenuation characteristics. On the other hand, the observed overestimation of the signal intensity in the anterior position for IQ-IRR underlines the importance of using corrections for scatter and attenuation for this cardio-centric system. In IQ-IRR-SC-AC, uniform signal intensity was obtained in the anterior, lateral, and posterior positions, resulting in  $IC$  values close to zero, but an unexpected underestimation of the signal intensity in the septal position was detected. When multifocal collimators are used, attenuation artifacts are position-dependent and are expected to be more pronounced than with LEHR collimators [13]. Nevertheless, the non-uniformity of the signal intensity in the *LV* wall could be substantially corrected if the AC and SC are applied on image data obtained by the IQ SPECT device. The slight septal non-uniformity of the signal intensity could be a result of the application of the AC that seems to overcorrect values in the septal position.

The *MPI system* and *PD* position were both found to be the main effects on  $NC$ . Lesion position has a dominant effect on the  $NC$  variability. IQ-IRR-SC-AC and SPECT-IRR-SC were found to have the largest  $NC$  mean values overall, with the differences not being statistically significant. SPECT-IRR had lower  $NC$  mean values than IQ-IRR-SC-AC and SPECT-IRR-SC. The differences were not statistically significant, mainly due to the relatively large variation in the results determined with SPECT-IRR. SPECT-IRR also performed similarly to IQ-IRR, with differences that were not statistically significant. Therefore, if least-squares average values are considered, IQ-IRR performs similar to SPECT-IRR (Figure 5). Nevertheless, substantial differences in the  $NC$  values at different *PD* positions were noted between IQ-IRR and SPECT-IRR (Figure 6). For IQ-IRR, the  $NC$  values were uniform for anterior, lateral, and septal positions, while a decrease of up to 15% for the posterior position was observed due to a loss of sensitivity with multifocal collimators in the area farthest from the detector. It is also interesting to note that in the anterior and lateral positions, there was no difference between IQ-IRR-SC-AC and IQ-IRR in terms of  $NC$  values. On the contrary, in the posterior and septal positions, corrections made a difference, enabling an improved perfusion detection capability of the cardio-centric system in these areas highly influenced by attenuation and scatter contribution. Attenuation artifacts that are more pronounced for multifocal collimators could be corrected if AC is applied. In SPECT-IRR-SC, an increase in the mean  $NC$  values for the lateral, posterior, and septal positions is visible compared to those for SPECT-IRR. Concerning the effect of lesion position on  $NC$ , the posterior position was found to produce the lowest values with statistically significant differences between the posterior and all other lesion positions (Figure 7). Even though the correction due to the intrinsic contrast was considered in the calculation of the  $NC$  (Equation (7)), the perfusion detection capability of *MPI systems* in the posterior part of the heart is still the lowest. The

results for *NC* obtained in this study can be used as reference values of the maximum contrast between the *PD* and *LV* wall.

In this investigation, a set of physical descriptors related to image contrast were used for the characterization of different imaging device–reconstruction algorithm–correction combinations. Once image quality is evaluated, advanced features can be implemented to optimize SPECT procedures with the use of convolutional neural networks [22–25]. IQ SPECT technology with the IRR algorithm may produce better spatial resolution, contrast, and sensitivity. Consequently, such *MPI systems* provide the possibility for the reduction of acquisition time or administered activity. This calls for a revision of practice and national diagnostic reference levels for respective nuclear medicine diagnostic procedures [26].

## 5. Limitations

The static phantom used in this study allows the evaluation of ungated SPECT image data. The next step in this investigation will be to conduct simulations of clinical conditions with a Monte Carlo-based algorithm and an advanced dynamic phantom to perform a full characterization. In this way, the dynamic simulation of electrocardiographically gated myocardial perfusion SPECT (GSPECT) will be performed. Additionally, the purpose of this investigation was to evaluate the perfusion detection capability of *MPI systems* simulating clinical conditions. For that reason, acquisition and reconstruction parameters used routinely in clinical studies were used (Table 1).

## 6. Conclusions

The characteristics of myocardial perfusion imaging devices and reconstruction algorithms necessitate a comprehensive image quality evaluation of *MPI systems*. The results of the image analysis of selected image quality descriptors in both normal and pathological heart simulations showed the intrinsic characteristics of the evaluated systems. An extended quantitative evaluation of the self-attenuation and perfusion detection capability of different *MPI systems* was performed concerning intrinsic contrast and net contrast. This investigation revealed minimal self-attenuation artifacts and better signal uniformity in the *LV* wall over all short-axis images when IQ-IRR-SC-AC was used ( $IC < 1\%$  for anterior, lateral, and posterior positions), except for the septal position. In the latter, an underestimation of the signal intensity was observed, resulting in an unexpectedly higher intrinsic contrast value in the septal part of the heart ( $2.38 \pm 0.53\%$ ). Concerning the perfusion detection capability, the net contrast values for the *MPI systems* were found to be perfusion-defect-position-dependent:  $32.09 \pm 2.05\%$ ,  $28.80 \pm 2.13\%$ ,  $21.64 \pm 2.21\%$ , and  $35.13 \pm 3.57\%$ , for anterior, lateral, posterior, and septal positions, respectively. The results show that IQ-IRR-SC-AC and SPECT-IRR-SC have the highest net contrast means overall at  $31.11 \pm 3.22\%$  and  $30.97 \pm 2.75\%$ , respectively. In the case of IQ-IRR-SC-AC, it was found that corrections made a difference in the posterior and septal positions when evaluating net contrast ( $26.61\%$  and  $39.07\%$  for IQ-IRR-SC-AC vs.  $14.03\%$  and  $30.78\%$  for IQ-IRR). This fact enables better perfusion detection capability over all short-axis images of IQ-IRR-SC-AC and minimizes the lack of perfusion detection capability for that particular *MPI system* in the posterior part of the heart, which is present otherwise. A substantial deterioration in image data quality was observed for IQ-IRR compared to IQ-IRR-SC-AC, and the performance could be compared to SPECT-IRR. The results of this investigation suggest that there is also a gain in terms of image quality and perfusion detection capability from the use of a double-energy window in SPECT devices with IRR for scatter correction ( $C_{LV/LVIC}$ :  $57.43 \pm 2.87\%$  and  $63.76 \pm 2.87\%$  for SPECT-IRR and SPECT-IRR-SC, respectively; *NC*:  $27.40 \pm 4.50\%$  and  $30.97 \pm 2.75\%$  for SPECT-IRR and SPECT-IRR-SC, respectively).

The results of the comprehensive evaluation of *MPI systems* using the standard phantom presented in this study will be used as reference values in further research.

**Author Contributions:** Conceptualization, D.D.D., R.M. and S.J.; Investigation, D.D.D.; Methodology, D.D.D., R.M. and S.J.; Validation, D.D.D.; Data curation, D.D.D. and I.P.; Formal analysis, D.D.D. and I.P.; Resources, S.J.; Visualization, D.D.D.; Project administration, D.D.D. and S.J.; Resources, S.J.; Writing—Original draft, D.D.D.; Writing—Review and editing, D.D.D., R.M., S.J., M.B. and I.P. Supervision, S.J. and R.M. All authors have read and agreed to the published version of the manuscript.

**Funding:** Part of the investigation was performed within the scope of the projects IAEA CRO6021 and UniRi-Iskusni-Prirod-23-8.

**Institutional Review Board Statement:** Not applicable.

**Informed Consent Statement:** Not applicable.

**Data Availability Statement:** The data presented in this study are available on request from the corresponding author. The data are not publicly available due to privacy.

**Conflicts of Interest:** The authors declare no conflicts of interest.

## References

- Zoccarato, O.; Scabbio, C.; De Ponti, E.; Matheoud, R.; Leva, L.; Morzenti, S.; Menzaghi, M.; Campini, R.; Marcassa, C.; Del Sole, A.; et al. Comparative Analysis of Iterative Reconstruction Algorithms with Resolution Recovery for Cardiac SPECT Studies. A Multi-center Phantom Study. *J. Nucl. Cardiol.* **2014**, *21*, 135–148. [[CrossRef](#)]
- Imbert, L.; Poussier, S.; Franken, P.R.; Songy, B.; Verger, A.; Morel, O.; Wolf, D.; Noel, A.; Karcher, G.; Marie, P.-Y. Compared Performance of High-Sensitivity Cameras Dedicated to Myocardial Perfusion SPECT: A Comprehensive Analysis of Phantom and Human Images. *J. Nucl. Med.* **2012**, *53*, 1897–1903. [[CrossRef](#)]
- Liu, C.J.; Cheng, J.S.; Chen, Y.C.; Huang, Y.H.; Yen, R.F. A Performance Comparison of Novel Cadmium-Zinc-Telluride Camera and Conventional SPECT/CT Using Anthropomorphic Torso Phantom and Water Bags to Simulate Soft Tissue and Breast Attenuation. *J. Nucl. Med.* **2015**, *29*, 342–350. [[CrossRef](#)]
- Hosny, T.; Khalil, M.M.; Elfiky, A.A.; Elshemey, W.M. Image Quality Characteristics of Myocardial Perfusion SPECT Imaging Using State-Of-The-Art Commercial Software Algorithms: Evaluation of 10 Reconstruction Methods. *Am. J. Nucl. Med. Mol. Imaging.* **2020**, *15*, 375–386.
- Enevoldsen, L.H.; Menashi, C.A.; Andersen, U.B.; Jensen, L.T.; Henriksen, O.M. Effects of Acquisition Time and Reconstruction Algorithm on Image Quality, Quantitative Parameters, and Clinical Interpretation of Myocardial Perfusion Imaging. *J. Nucl. Cardiol.* **2013**, *20*, 1086–1092. [[CrossRef](#)]
- Mezzenga, E.; Sarnelli, A.; Bellomo, G.; DiFilippo, F.P.; Palestro, C.J.; Nichols, K.J. Quantification of SPECT Concentric Ring Artifacts by Radiomics and Radial Features. *Appl. Sci.* **2022**, *12*, 2726. [[CrossRef](#)]
- Ke, C.-H.; Liu, W.-J.; Peng, B.-R.; Pan, L.-F.; Pan, L.-K. Optimizing the Minimum Detectable Difference of Gamma Camera SPECT Images via the Taguchi Analysis: A Feasibility Study with a V-Shaped Slit Gauge. *Appl. Sci.* **2022**, *12*, 2708. [[CrossRef](#)]
- Caobelli, F.; Ren Kaiser, S.; Thackeray, J.T.; Bengel, F.M.; Chieragato, M.; Soffientini, A.; Pizzocaro, C.; Savelli, G.; Guerra, U.P.; Galelli, M.; et al. The Importance of a Correct Positioning of the Heart Using IQ-SPECT System with Multifocal Collimators in Myocardial Perfusion Imaging: A Phantom Study. *J. Nucl. Cardiol.* **2015**, *22*, 57–65. [[CrossRef](#)]
- Nakajima, K.; Okuda, K.; Momose, M.; Matsuo, S.; Kondo, C.; Sarai, M.; Shibutani, T.; Onoguchi, M.; Shimizu, T.; Vija, A.H. IQ-SPECT Technology and its Clinical Applications Using Multicenter Normal Databases. *Ann. Nucl. Med.* **2017**, *31*, 649–659. [[CrossRef](#)] [[PubMed](#)]
- Caobelli, F.; Kaiser, S.R.; Thackeray, J.T.; Bengel, F.M.; Chieragato, M.; Soffientini, A.; Pizzocaro, C.; Savelli, G.; Galelli, M.; Guerra, U.P. IQ SPECT Allows a Significant Reduction in Administered Dose and Acquisition Time for Myocardial Perfusion Imaging: Evidence from a Phantom Study. *J. Nucl. Med.* **2014**, *55*, 2064–2070. [[CrossRef](#)] [[PubMed](#)]
- Vija, A.H.; Malmin, R.; Yahil, A.; Zeintl, J.; Bhattacharya, M.; Rempel, T.D.; Hawman, E.G.; Bendriem, B. A Method for Improving the Efficiency of Myocardial Perfusion Imaging Using Conventional SPECT and SPECT/CT Imaging Systems. In Proceedings of the IEEE Nuclear Science Symposium & Medical Imaging Conference, Knoxville, TN, USA, 30 October–6 November 2010. [[CrossRef](#)]
- Leva, L.; Matheoud, R.; Sacchetti, G.; Carriero, A.; Brambilla, M. Agreement between Left Ventricular Ejection Fraction Assessed in Patients with Gated IQ-SPECT and Conventional Imaging. *J. Nucl. Cardiol.* **2020**, *27*, 1714–1724. [[CrossRef](#)] [[PubMed](#)]
- Hyafil, F.; Gimelli, A.; Slart, R.H.J.A.; Georgoulas, P.; Rischpler, C.; Lubberink, M.; Sciagra, R.; Bucierius, J.; Agostini, D.; Verberne, H.J.; et al. EANM Procedural Guidelines for Myocardial Perfusion Scintigraphy using Cardiac-Centered Gamma Cameras. *Eur. J. Hybrid Imaging* **2019**, *3*, 11. [[CrossRef](#)] [[PubMed](#)]
- Brambilla, M.; Lecchi, M.; Matheoud, R.; Leva, L.; Lucignani, G.; Marcassa, C.; Zoccarato, O. Comparative Analysis of Iterative Reconstruction Algorithms with Resolution Recovery and New Solid State Cameras Dedicated to Myocardial Perfusion Imaging. *Phys. Medica* **2017**, *41*, 109–116. [[CrossRef](#)] [[PubMed](#)]

15. Knoll, P.; Kotalova, D.; Köchle, G.; Kuzelka, I.; Minear, G.; Mirzaei, S.; Sámal, M.; Zadrazil, L.; Bergmann, H. Comparison of Advanced Iterative Reconstruction Methods for SPECT/CT. *Z. Med. Phys.* **2012**, *22*, 58–69. [[CrossRef](#)] [[PubMed](#)]
16. Hawman, E.; Vija, A.H.; Daffach, R.; Ray, M. Flash 3D TM Technology Optimizing SPECT Quality and Accuracy. Order No. A91004-M2300-M102-01-7600. Printed in the U.S.A. PA06021. Available online: [https://www.researchgate.net/publication/265064101\\_Flash\\_3D\\_TM\\_Technology\\_Optimizing\\_SPECT\\_Quality\\_and\\_Accuracy](https://www.researchgate.net/publication/265064101_Flash_3D_TM_Technology_Optimizing_SPECT_Quality_and_Accuracy) (accessed on 29 June 2023).
17. Okuda, K.; Nakajima, K.; Yoneyama, H.; Shibutani, T.; Onoguchi, M.; Matsuo, S.; Hashimoto, M.; Kinuya, S. Impact of Iterative Reconstruction with Resolution Recovery in Myocardial Perfusion SPECT: Phantom and Clinical Studies. *Sci. Rep.* **2019**, *9*, 19618. [[CrossRef](#)]
18. Hutton, B.F.; Buvat, I.; Beekman, F.J. Review and Current Status of SPECT Scatter Correction. *Phys. Med. Biol.* **2011**, *56*, 85–112. [[CrossRef](#)] [[PubMed](#)]
19. Ichihara, T.; Ogawa, K.; Motomura, N.; Kubo, A.; Hashimoto, S. Compton Scatter Compensation Using the Triple-Energy Window Method for Single- and Dual-Isotope SPECT. *J. Nucl. Med.* **1993**, *34*, 2216–2221. [[PubMed](#)]
20. Zoccarato, O.; Marcassa, C.; Lizio, D.; Leva, L.; Lucignani, G.; Savi, A.; Scabbio, C.; Matheoud, R.; Lecchi, M.; Brambilla, M. Differences in Polar-Map Patterns Using the Novel Technologies for Myocardial Perfusion Imaging. *J. Nucl. Cardiol.* **2017**, *24*, 1626–1636. [[CrossRef](#)] [[PubMed](#)]
21. Zoccarato, O.; Matheoud, R.; Lecchi, M.; Scabbio, C.; Claudio, M.; Brambilla, M. Optimal <sup>99m</sup>Tc Activity Ratio in the Single-Day Stress-Rest Myocardial Perfusion Imaging Protocol: A Multi-SPECT Phantom Study. *J. Nucl. Cardiol.* **2021**, *28*, 338–349. [[CrossRef](#)]
22. Pribanić, I.; Simić, S.D.; Tanković, N.; Dundara Debeljuh, D.; Jurković, S. Reduction of SPECT Acquisition Time Using Deep Learning: A Phantom Study. *Phys. Medica* **2023**, *111*, 102615. [[CrossRef](#)]
23. Apostolopoulos, I.D.; Papathanasiou, N.D.; Papandrianos, N.; Papageorgiou, E.; Apostolopoulos, D.J. Innovative Attention-Based Explainable Feature-Fusion VGG19 Network for Characterising Myocardial Perfusion Imaging SPECT Polar Maps in Patients with Suspected Coronary Artery Disease. *Appl. Sci.* **2023**, *13*, 8839. [[CrossRef](#)]
24. Papandrianos, N.I.; Feleki, A.; Moustakidis, S.; Papageorgiou, E.I.; Apostolopoulos, I.D.; Apostolopoulos, D.J. An Explainable Classification Method of SPECT Myocardial Perfusion Images in Nuclear Cardiology Using Deep Learning and Grad-CAM. *Appl. Sci.* **2022**, *12*, 7592. [[CrossRef](#)]
25. Papandrianos, N.; Papageorgiou, E. Automatic Diagnosis of Coronary Artery Disease in SPECT Myocardial Perfusion Imaging Employing Deep Learning. *Appl. Sci.* **2021**, *11*, 6362. [[CrossRef](#)]
26. Dundara Debeljuh, D.; Jurković, S.; Pribanić, I.; Poljak, F.; Kralik, I.; Krstonošić, B.; Bralić, A.; Bajan, T.; Božac Jokić, O.; Vidošević, L.; et al. National Survey to Set Diagnostic Reference Levels in Nuclear Medicine Single Photon Emission Imaging in Croatia. *Phys. Medica* **2020**, *78*, 109–116. [[CrossRef](#)]

**Disclaimer/Publisher’s Note:** The statements, opinions and data contained in all publications are solely those of the individual author(s) and contributor(s) and not of MDPI and/or the editor(s). MDPI and/or the editor(s) disclaim responsibility for any injury to people or property resulting from any ideas, methods, instructions or products referred to in the content.